Special multicolor illumination and numerical tilt correction in volumetric digital holographic microscopy

Márton Zsolt Kiss,[1,2,*] Benedek J. Nagy,[3] Péter Lakatos,[2] Zoltán Göröcs,[1] Szabolcs Tőkés,[2] Balázs Wittner,[1] and László Orzó[1]

[1]*Cellular Sensory and Wave Computing Laboratory, Institute for Computer Science and Control, Hungarian Academy of Sciences H-1111 Budapest, Hungary*
[2]*Faculty of Information Technology and Bionics, Pázmány Péter Catholic University H-1083 Budapest, Hungary*
[3]*Wigner Research Centre for Physics, Hungarian Academy of Sciences H-1121 Budapest, Hungary*
[*]*kiss.marton@sztaki.mta.hu*
http://www.analogic.sztaki.hu

Abstract: We introduce a color imaging method in our digital holographic microscope system (DHM). This DHM can create color images of freely floating, or moving objects inside a large volume by simultaneously capturing three holograms using three different illumination wavelengths. In this DHM a new light source assembly is applied, where we use single mode fibers according to the corresponding wavelengths that are tightly and randomly arranged into a small array in a single FC/PC connector. This design has significant advantages over the earlier approaches, where all the used illuminations are coupled in the same fiber. It avoids the coupling losses and provides a cost effective, compact solution for multicolor coherent illumination. We explain how to determine and correct the different fiber end positions caused tilt aberration during the hologram reconstruction process. To demonstrate the performance of the device, color hologram reconstructions are presented that can achieve at least 1 μm lateral resolution.

OCIS codes: (090.1995) Digital holography; (100.2000) Digital image processing; (100.3010) Image reconstruction techniques; (180.3170) Interference microscopy.

References and links

1. D. Gábor, "A new microscopic principle," Nature **161**(4098), 777–778 (1948).
2. P. Hariharan, *Optical Holography: Principles, Techniques and Applications* (Cambridge University, 1996), Vol. 20.
3. U. Schnars and W. Jueptner, *Digital holography* (Springer, 2005).
4. C. Mann, L. Yu, C.-M. Lo, and M. Kim, "High-resolution quantitative phase-contrast microscopy by digital holography," Opt. Express **13**(22), 8693–8698 (2005).
5. J. Garcia-Sucerquia, W. Xu, S. K. Jericho, P. Klages, M. H. Jericho, and H. J. Kreuzer, "Digital in-line holographic microscopy," Appl. Opt. **45**(5), 836–850 (2006).
6. Z. Göröcs and A. Ozcan, "On-chip biomedical imaging," IEEE Rev. Biomed. Eng. **6**, 29–46 (2013).
7. T. Shimobaba, Y. Sato, J. Miura, M. Takenouchi, and T. Ito, "Real-time digital holographic microscopy using the graphic processing unit," Opt. Express **16**(16), 11776–11781 (2008).
8. L. Orzó, Z. Göröcs, I. Szatmári, and S. Tőkés, "Gpu implementation of volume reconstruction and object detection in digital holographic microscopy," in "Cellular Nanoscale Networks and Their Applications (CNNA), 2010 12th International Workshop on," (IEEE, 2010), pp. 1–4.
9. T. Shimobaba, J. Weng, T. Sakurai, N. Okada, T. Nishitsuji, N. Takada, A. Shiraki, N. Masuda, and T. Ito, "Computational wave optics library for C++: CWO++ library," Comput. Phys. Commun. **183**(5), 1124–1138 (2012).
10. A. F. Coskun, T.-W. Su, and A. Ozcan, "Wide field-of-view lens-free fluorescent imaging on a chip," Lab Chip **10**(7), 824–827 (2010).
11. W. Bishara, T.-W. Su, A. F. Coskun, and A. Ozcan, "Lensfree on-chip microscopy over a wide field-of-view using pixel super-resolution," Opt. Express **18**(11), 11181–11191 (2010).
12. J. Kühn, F. Charrière, T. Colomb, E. Cuche, F. Montfort, Y. Emery, P. Marquet, and C. Depeursinge, "Axial sub-nanometer accuracy in digital holographic microscopy," Meas. Sci. Technol. **19**(7), 074007 (2008).

#203656 - $15.00 USD Received 26 Dec 2013; revised 5 Feb 2014; accepted 8 Feb 2014; published 25 Mar 2014

13. P. Marquet, B. Rappaz, P. J. Magistretti, E. Cuche, Y. Emery, T. Colomb, and C. Depeursinge, "Digital holographic microscopy: a noninvasive contrast imaging technique allowing quantitative visualization of living cells with subwavelength axial accuracy," Opt. Lett. **30**(5), 468–470 (2005).
14. I. Yamaguchi, J. Kato, S. Ohta, and J. Mizuno, "Image formation in phase-shifting digital holography and applications to microscopy," Appl. Opt. **40**(34), 6177–6186 (2001).
15. T. Colomb, J. Kühn, F. Charrière, C. Depeursinge, P. Marquet, and N. Aspert, "Total aberrations compensation in digital holographic microscopy with a reference conjugated hologram," Opt. Express **14**(10), 4300–4306 (2006).
16. S. Yeom, I. Moon, and B. Javidi, "Real-time 3-D sensing, visualization and recognition of dynamic biological microorganisms," Proc. IEEE **94**(3), 550–566 (2006).
17. I. Moon, M. Daneshpanah, B. Javidi, and A. Stern, "Automated three-dimensional identification and tracking of micro/nanobiological organisms by computational holographic microscopy," Proc. IEEE **97**(6), 990–1010 (2009).
18. L. Repetto, F. Pellistri, E. Piano, and C. Pontiggia, "Gabor's hologram in a modern perspective," Am. J. Phys. **72**(7), 964–967 (2004).
19. Z. Göröcs, M. Kiss, V. Tóth, L. Orzó, and S. Tőkés, "Multicolor digital holographic microscope (DHM) for biological purposes," in "BiOS," (International Society for Optics and Photonics, 2010), p. 75681P.
20. Z. Göröcs, L. Orzó, M. Kiss, V. Tóth, and S. Tőkés, "In-line color digital holographic microscope for water quality measurements," in "Laser Applications in Life Sciences 2010," (International Society for Optics and Photonics, 2010), p. 737614.
21. W. Xu, M. H. Jericho, I. A. Meinertzhagen, and H. J. Kreuzer, "Digital in-line holography for biological applications," Proc. Natl. Acad. Sci. U.S.A. **98**(20), 11301–11305 (2001).
22. A. Greenbaum, A. Feizi, N. Akbari, and A. Ozcan, "Wide-field computational color imaging using pixel super-resolved on-chip microscopy," Opt. Express **21**(10), 12469–12483 (2013).
23. A. Greenbaum, N. Akbari, A. Feizi, W. Luo, and A. Ozcan, "Field-portable pixel super-resolution colour microscope," PLoS ONE **8**(9), e76475 (2013).
24. F. Shen and A. Wang, "Fast-Fourier-transform based numerical integration method for the Rayleigh-Sommerfeld diffraction formula," Appl. Opt. **45**(6), 1102–1110 (2006).
25. L. Repetto, E. Piano, and C. Pontiggia, "Lensless digital holographic microscope with light-emitting diode illumination," Opt. Lett. **29**(10), 1132–1134 (2004).
26. O. Mudanyali, D. Tseng, C. Oh, S. O. Isikman, I. Sencan, W. Bishara, C. Oztoprak, S. Seo, B. Khademhosseini, and A. Ozcan, "Compact, light-weight and cost-effective microscope based on lensless incoherent holography for telemedicine applications," Lab Chip **10**(11), 1417–1428 (2010).
27. J. Alda, *Laser and Gaussian Beam Propagation and Transformation*, Encyclopedia of Optical Engineering (Taylor & Francis, 2007).
28. W. Bishara, U. Sikora, O. Mudanyali, T.-W. Su, O. Yaglidere, S. Luckhart, and A. Ozcan, "Holographic pixel super-resolution in portable lensless on-chip microscopy using a fiber-optic array," Lab Chip **11**(7), 1276–1279 (2011).
29. H.-J. Cho, D.-C. Kim, Y.-H. Yu, S. Shin, and W. Jung, "Tilt aberration compensation using interference patterns in digital holography," J. Opt. Soc. Korea **13**(4), 451–455 (2009).
30. E. Cuche, P. Marquet, and C. Depeursinge, "Aperture apodization using cubic spline interpolation: application in digital holographic microscopy," Opt. Commun. **182**(1-3), 59–69 (2000).
31. K. Matsushima and T. Shimobaba, "Band-limited angular spectrum method for numerical simulation of free-space propagation in far and near fields," Opt. Express **17**(22), 19662–19673 (2009).
32. J. W. Goodman, *Introduction to Fourier Optics* (Roberts and Company Publishers, 2005).
33. P. Ferraro, S. Grilli, L. Miccio, D. Alfieri, S. De Nicola, A. Finizio, and B. Javidii, "Full color 3-D imaging by digital holography and removal of chromatic aberrations," J. Displ. Technol. **4**(1), 97–100 (2008).
34. A. E. Siegman, *Lasers University Science Books* (Mill Valley, 1986), Vol. 37.

1. Introduction

Based on Gabor's pioneering invention [1], holographic principles were attempted to apply in microscopy in a number of times [2]. The research in this field was outstandingly accelerated [3] when silver halide films, which were conventionally used for hologram recording, were replaced by commercial digital cameras (CCD or CMOS area scan sensors). Although there is no more need of the slow wet-chemical development process, the achievable resolution is limited in this case by the number and size of the pixels of the applied digital sensor. Therefore, it usually seems indispensable to apply special Digital Holographic Microscope (DHM) architectures, where the hologram of the magnified object can satisfy the Nyquist constraints [4] on the sensor surface. However, there are lensless DHM approaches too [5, 6]. In Digital Holography the reconstructions are calculated digitally from the recorded holograms using wave field propagation algorithms. Current high speed computers, particularly the emerging parallel computing architectures (e.g. GPU), make it possible to achieve close to real time reconstruction speed [7–9].

#203656 - $15.00 USD Received 26 Dec 2013; revised 5 Feb 2014; accepted 8 Feb 2014; published 25 Mar 2014

The utilization of a DHM is promising for several reasons: First of all, it can provide simple, low-cost, lensless microscope architectures [10, 11], that can achieve high quality reconstructions at fair resolution. Even sub-nanometer axial resolution [12, 13] can be achieved by the application of appropriate off-axis (or on-axis with phase shifting interferometry [14]) DHM architectures. In this case, even the aberrations of the applied optics can be corrected efficiently [15] during the hologram reconstruction process. Ultimately, DHM seems to be extremely suitable to implement volumetric imaging. A single hologram can record the diffraction of all the objects within the illuminated and observed volume, and later, based on these data each of these objects can be reconstructed [16, 17]. This way, for sparse samples, which is a requirement in Gabor in-line holography [18], it becomes feasible to reconstruct objects at high resolution from a really large volume.

Using the holographic volumetric imaging technique we have developed a DHM [19, 20] for biological water quality monitoring purposes. It is able to determine microbiological content (algae and worms) of the natural and drinking water samples automatically. These data can be efficiently used to monitor the microorganisms in natural water bodies, and to characterize the quality of the filtration process in water wells [19, 20].

Our DHM setup records high resolution Gabor-type [1, 21] in-line holograms, as it utilize the space bandwidth product more efficiently than the other architectures [20]. Using a single recorded hologram we are able to inspect orders of magnitude larger volume compared to approaches that applies conventional microscopy [5] where the depth of focus is constrained considerably by the requested lateral resolution. An afocal optical system is applied in the DHM (see in Fig. 1) that makes uniform magnification reconstructions available within the whole observed volume even if the planar illumination is not guaranteed.

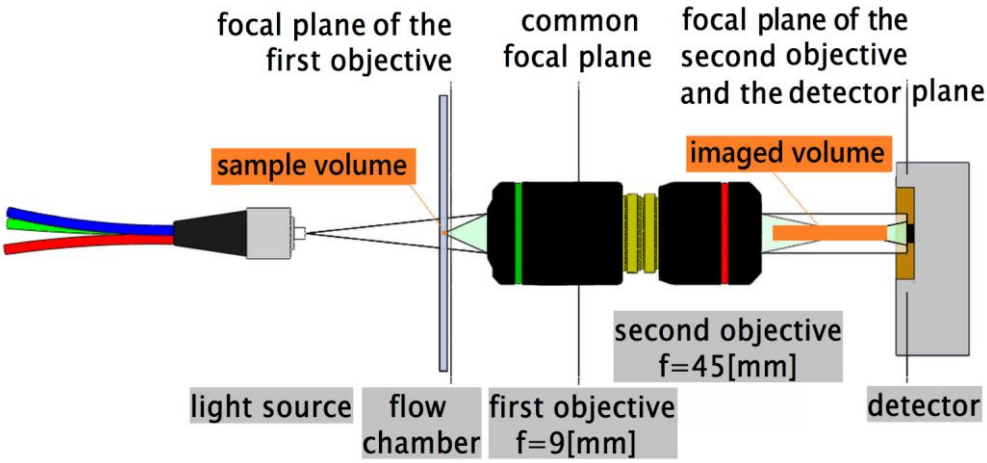

Fig. 1. Our multicolor DHM setup aims to reconstruct the image of freely floating objects within the volume of a flow through chamber. Application of an afocal optical setup provides uniform (5 times lateral and 25 times longitudinal) magnification within the whole observed volume. The red, green, and blue holograms are simultaneously acquired by a detector using Bayern-pattern color filter, while the illumination is provided by synchronized flashes of the applied lasers.

Color information is usually indispensable to correctly discriminate the observed objects, e.g. different types of algae. Therefore, in our DHM device color image of the object is reconstructed from the simultaneously captured holograms of three different (red 650 nm, green 532 nm, and blue 473 nm) wavelengths. These in-line holograms are formed by a common afocal optical setup and by the application of appropriate, coherent, multicolor illumination, while it is captured by an area scan (CMOS) sensor using a Bayer-pattern color filter [19]. As the examined objects can move within the sample volume, therefore we are not able to use the approaches, where the high resolution color images of the objects are reconstructed from several, sequentially captured, different color holograms [22, 23].

#203656 - $15.00 USD Received 26 Dec 2013; revised 5 Feb 2014; accepted 8 Feb 2014; published 25 Mar 2014

In our DHM the angular spectrum method [24] is applied at the reconstruction. It works for small propagation distances and does not apply any approximation.

To ensure high resolution, accurate hologram reconstructions we have to use regular, even illuminating (reference) wave fields. We use digital replicas of the illuminating reference wave fields to implement correct digital hologram reconstruction in the DHM. All the neglected irregularities of the illuminating reference wave field causes mis-assessment of the reconstructing wave field and results in the distortions of the reconstructions.

Single mode optical fibers can provide high quality illuminating reference wave fields. Earlier, we applied fiber couplers to provide the required multicolor coherent illumination [19]. However, that solution had some serious drawbacks: considerable light losses, expensive optical elements, and it is hard to ensure that the final common fiber would be optimal for all the applied wavelengths. Therefore, to improve the quality of the illuminating reference wave fields, we have developed a new type of multicolor illuminating assembly. This design provides high quality single mode illuminating laser beams at (e.g. three) different wavelengths, by collecting the individual, wavelength tuned single mode optical fibers, while the ends of these fibers are tightly bundled into the same connector.

This new kind of device provides high quality, regular wave fields for all the applied wavelengths, but due to the special design it causes some position dependent misalignments into the color hologram reconstructions. We analyzed these errors and found that the small displacement of the illuminating light sources causes some kind of tilt aberration among the different color hologram reconstructions. We have developed a simple method that can compensate this tilt effects efficiently.

Our work is organized as follows: In Section 2, we delineate our new coherent illuminating design and detail its advantages, disadvantages. In Section 3, we analyze the tilt caused by the applied new illumination and provide an algorithm for its efficient numerical correction. First, we analyze the effects of the exact illuminating light source positions on the shifts of the reconstructed images. Next, we provide a simple numerical method, using reconstructing beams of properly set inclination angles to compensate the introduced tilt aberrations. We compare the analytically calculated and also the measured shifts in the case of a lensless in-line holographic setup and in our DHM. We offer a simple modification of the tilt compensation parameters to avoid the appearance of artificial diffraction fringes caused by the tilted reconstruction beams phase discontinuity at the hologram boundaries. Finally, in Section 4, we demonstrate the performance of the DHM device that applies the introduced new illumination and the corresponding tilt corrections by some reconstructed color algae images.

2. Coherent multicolor illumination implementation in the DHM

Applying a DHM, our principal aim is to monitor a large volume of fluid samples (of up to 1.5 mm depth, 1 mm^2 field of view) at high (1 μm lateral) resolution. To implement an in-line holographic microscope—like our DHM approach—we need an illuminating light source that has the required coherence and an even, regular, high quality (spherical or planar) wave field that can be correctly generated digitally during the numerical hologram reconstruction process.

For high resolution, volumetric, holographic imaging the application of led based illuminations [25] is not satisfactory, even if they are placed far from the sample [26], due their small coherence lengths. However, applying affordable laser light sources, it is easy to assure coherence lengths that do not limit the effective numerical apertures of the object, the interference of the object diffractions, and the illuminating reference wave field at the hologram plane any more. A Gaussian laser beam, far from its waist can be fairly approximated locally by uniform, smooth spherical or planar wave fields [27]. We can get such a Gaussian beam profile from almost any kind of laser sources—even from low cost (diode) lasers—by the application of spatial frequency filtering. Although, using an appropriate pinhole as spatial filter [21] can provide a high quality wave field, it is usually accompanied by huge light intensity loss. As usually a high numeric aperture microscope

#203656 - $15.00 USD Received 26 Dec 2013; revised 5 Feb 2014; accepted 8 Feb 2014; published 25 Mar 2014

objective is applied to focus the light in the pinhole, this type of implementation of the spatial frequency filtering and the required adjustments are troublesome and expensive. Such a design is sensitive to the displacements or dilatations of the elements of the device: e.g. a few micrometer shift of the illumination (considering a one micron diameter pinhole) can produce tremendous light losses. Dust or dirt can easily clog the pinhole that is hard to avoid during the long term use of the setup. Furthermore, the cleaning of a clogged pinhole is a challenging task. Implementing multicolor illumination using pinholes seems to be a really difficult task. Therefore, we apply another method, where the lasers are coupled into single mode fibers. Fiber coupled lasers can provide high quality Gaussian beams of the required, predefined parameters and avoid the above detailed shortcomings of the pinhole based techniques. Using such laser fibers it is much simpler to guide and position the laser beams.

To provide proper illumination in our color DHM, previously we coupled the light of the applied three different fiber coupled lasers into the same optical fiber using special fiber couplers [19, 20]. Although this type of coupling is simple and straightforward, it has severe shortcomings: First of all, the couplings are usually accompanied by considerable light losses. Also, the efficient single-mode operation is hard to ensure for all the three coupled wavelengths in the final common fiber. Finally, the commercially available fiber couplers are expensive.

To avoid these limitations, we introduce a simple, new fiber coupling construct, where the stripped, single mode, randomly but parallel arranged fiber ends are tightly packed in a single fiber connector. The mutual distances of the cores in this construct are limited by the diameter of the individual claddings (in our case it is 125 μm). In this new type of construct the overlapping, common section of the emerging light cones can be used for "white light" illumination. This construction is depicted in Fig. 2.

Although, there can be other laser holder constructions that can replace this design [28], but the cleaning, and polishing would be much harder to solve in those designs.

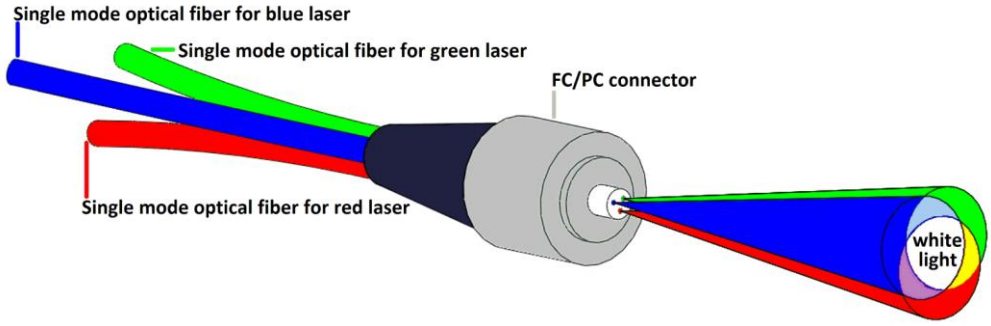

Fig. 2. In the introduced special illuminating light source the three different fiber ends are tightly packaged in the same connector. Near the axis where the beams overlap, we can get "white light" illumination, with RGB line spectrum.

To get a correct color image from the red, green, and blue reconstructions, these monochromatic images should represent the same views of the same object. This is the reason why it is necessary to illuminate the target objects from almost the same direction in different colors. It is satisfied in our case as the view angles of the fiber ends from any target points are smaller than 0.1 degree.

Our new design provides multicolor illumination by simple combination of several single mode Gaussian beams. It does not require the use of fiber couplers; it is flexible, robust, and provides more stable, cheaper illumination than the previous approaches. It can be assembled in any optical laboratory, using a simple fiber optic connectorization kit.

3. Multicolor hologram reconstruction

As we mentioned in the introduction the neglected, undetected irregularities of the illuminating reference wave field will result distortions at the reconstructed objects. Since we

#203656 - $15.00 USD Received 26 Dec 2013; revised 5 Feb 2014; accepted 8 Feb 2014; published 25 Mar 2014

use single mode fiber ends that provides regular, high quality Gaussian beams, these distortions are minimal. However, the different color illuminations have distinct positions in our new device and this can introduce some aberrations of the reconstruction too.

3.1 Effects of the illumination arrangement and its compensation

Our experiments show that the simulated propagation of the different color holograms to achieve reconstructions causes a few pixel displacements of the different color reconstructions of the same object. Furthermore, there is linear relationship between the observed size of the displacement and the applied reconstruction distance. Although the illuminating reference and reconstructing wave fields are similar but they have different propagation directions that causes the displacement of the reconstructed image position. Therefore, if we choose appropriate reconstruction beam direction, the reconstructed image of an object will be shifted in its proper, original position.

In our multicolor DHM setup, as the position of the light sources are not the same, they illuminate the detector from slightly different directions. That is, the illuminating reference wave fields, corresponding to the different colors, have different angles of incidence. Therefore, if we apply the same direction for the reconstructing wave fields of the different color hologram reconstructions, we introduce some bias that can be considered as some kind of tilt aberration. In Fig. 3 it is depicted, how the different color illuminating reference beams reach the detector.

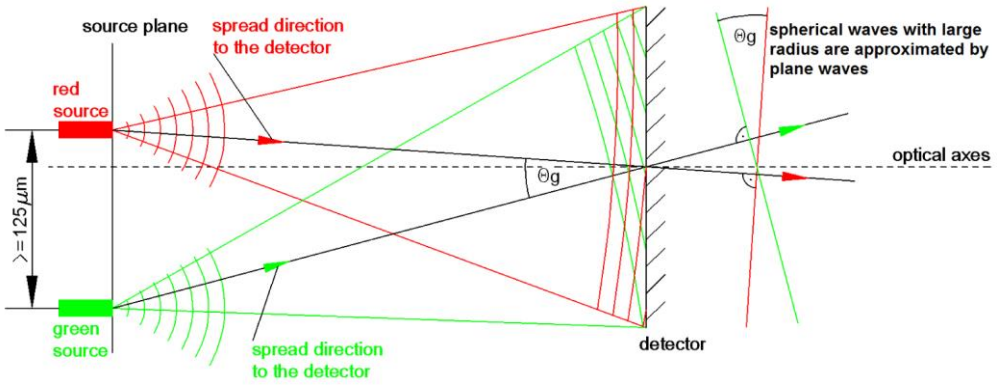

Fig. 3. As in the new illumination design the light sources are slightly displaced (~125 μm), the corresponding illuminating reference wave fields - which can be approximated by plane waves - have different incident direction at the detector.

It can be easily recognized that the relative directions of the illuminating reference and reconstruction beam define the positions of the reconstructed image of the objects. This is not really important if we consider a single hologram reconstruction as it results in a slightly rotated reconstruction of the volume. However, if we have different color holograms, it can easily cause misalignments between the color reconstructions of the same object. Our novel illumination design is not the only one that can introduce this type of bias, but also other multicolor illumination designs can suffer from it, where the different colors are coupled by semi transparent or dichroic mirrors and the perfect alignment is not ensured.

Adjusting the propagation direction of the different color reconstructing wave fields — let us call it tilt compensation [29] — the color images of the reconstructed object can be realigned. Measuring the relative shift of the reconstructions of two different holograms, we can define the inclination angle of the reconstructing beam that can compensate it perfectly. We use a distant, small, black object to define the proper inclination angels for the different colors. Applying these gained parameters we become able to compensate the shift of the reconstructions independently of the place of the object within the whole volume.

#203656 - $15.00 USD Received 26 Dec 2013; revised 5 Feb 2014; accepted 8 Feb 2014; published 25 Mar 2014

3.2 Relationship between the illumination geometry and the introduced tilt aberration

We used theoretical calculations and measurements to estimate the effects of the diverse positions of the illuminating laser fiber ends on the introduced tilt aberration. We approximated the illumination wave fields as Gaussian beams with waist center at different distances from the optical axis, while their distances from the detector are the same. We applied the ray transfer matrix (ABCD) of the optical setup on these decentered Gaussian beams [27]. Based on this calculation we defined the complex wave fields of the axial and the displaced Gaussian beams at the hologram plane and estimated the amount of tilt that has been introduced by them. Details of the calculation can be found in the Appendix.

In the first measurement, a lensless, monochrome experimental optical setup was used, where we compared the measured and the estimated tilts. We were searching for the proper tilt angle of the reconstructing wave field, which ensures that the position of the reconstruction is the same as it would be without the displacement of the fiber laser end. The first (reference) position was set by placing the laser fiber end in the optical axis and no tilt is applied for the reconstruction. We used a red (650 nm) fiber coupled laser and the steps of the displacements of the fiber end were 150 µm (the laser-object and the object-sensor distances were 100 mm and 23 mm respectively).

We have also made analytical calculations to estimate tilt differences based on the application of the ABCD formalism on decentered Gaussian beams. The comparison of the measured data and results of the analytical calculations is shown in Fig. 4.

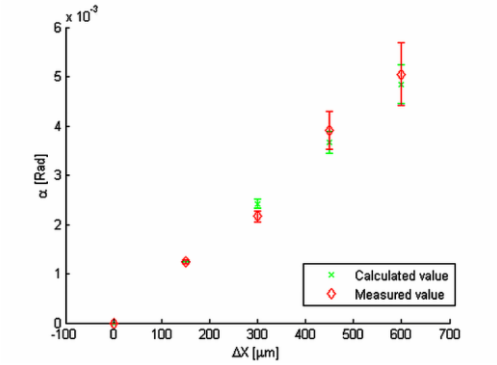

Fig. 4. The calculated and the measured tilts depending on the displacement of the laser light source from the optical axis.

We can observe good match of the measured and calculated data. The remaining differences are probably caused by the position measurement inaccuracies of the reconstructed object.

As the applied light source displacements (ΔX) are small, they are directly proportional with the tilt of the illuminating reference beam. We found linear relationship between the tilts of the physical reference and the numerical reconstruction (α) beams. Through this measurement we were able to show that the fiber end displacement causes tilt aberration.

In the second measurement, we analyzed the new illumination device caused tilts using the parameters of our multicolor DHM optical setup. The position of the hologram reconstruction depends only on the angle between the applied illuminating reference and reconstruction beams. Therefore the introduced tilt aberration is defined by the relative position of the illumination source and the sensor surface (transformed by the applied optical setup) and eventually does not depend on the actual 3D position of the objects. As we mentioned above, for correct tilt compensation we need only the relative tilts (like θ_g in Fig. 3.). Therefore, we can use one of the illuminating beams as reference direction.

Fortunately, all the required parameters of the optical setup (e.g. focal lengths of the applied objectives, sensor position, position of the illumination etc.) are known. This way, we

#203656 - $15.00 USD Received 26 Dec 2013; revised 5 Feb 2014; accepted 8 Feb 2014; published 25 Mar 2014

determined how the afocal optical system shifts the virtual position of the light sources (see in Fig. 5).

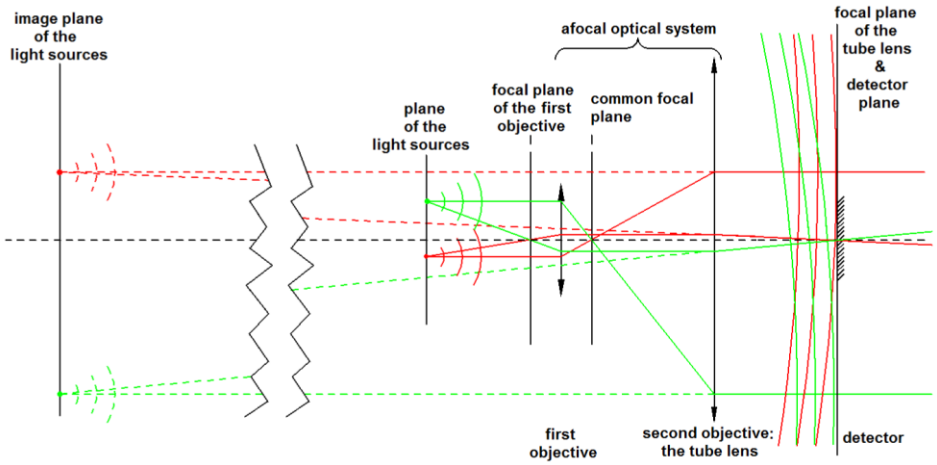

Fig. 5. Our afocal optical system magnifies the distances between the fiber ends (the red and the green points) and transposes the virtual position of the light sources in much larger distance from the detector. Therefore the Gaussian beams can be correctly approximated by (tilted) plane waves at the detector surface.

The directions of the Gaussian beams leaving the fiber ends are considered to be parallel to the optical axis. With the use of special fiber optic inspection microscope we recorded the photo of the connector (see in Fig. 6.) and based on these data we measured the distances of the individual fiber ends. The three circles are corresponding to the 125 μm diameter claddings of the different cores.

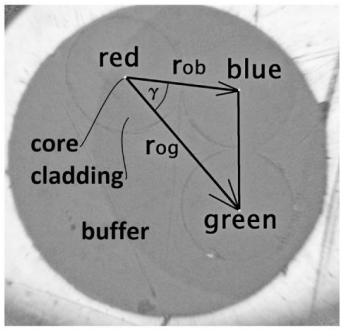

Fig. 6. Photograph of the fiber connector end, incorporating the three different single mode fiber ends. The black arrows indicate the distances between the red and green, and red and blue fiber ends.

Based on the different color hologram reconstructions we *measured* the relative tilts of the green and blue reconstruction beams to the red one. Also we have made *calculations about* the same relative tilts based on the fiber end position data (r_{og} and r_{ob} distances, and γ) and the actual optical setup parameters using the ABCD formalism. The calculated and the measured relative tilt angles (Θ) of the red–green and red–blue beams show proper matching, while the difference angle of the red–green and red–blue directions (γ) determined by the reconstruction shifts and by the fiber end position data are fitting well too (see in **Table 1**).

#203656 - $15.00 USD Received 26 Dec 2013; revised 5 Feb 2014; accepted 8 Feb 2014; published 25 Mar 2014

Table 1. The relative tilt angles (Θ) of the calculated (related to the illuminating reference beams) and the measured (related to the reconstruction beams) data are shown here. γ shows the angle between the red-blue and red-green light axes defined planes.

λ [nm]	r_0 [μm]	Θ [rad]		γ [rad]	
		calculated	measured	calculated	measured
650	0	0	0	0.747	0.728
473	r_{ob} = 130	0.000591	0.000545		
532	r_{og} = 195	0.000886	0.000790		

Appropriate tilt compensation realign the different color hologram reconstructions into matching positions and produce proper color image (see in Fig. 7)

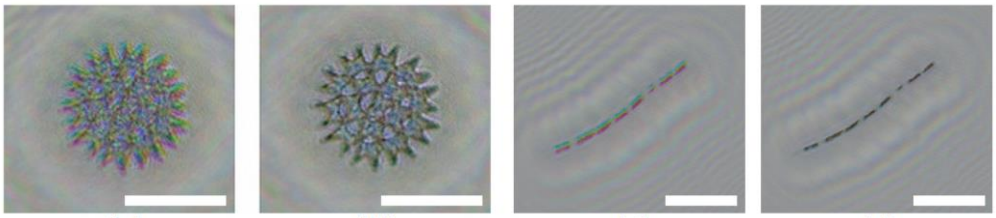

Fig. 7. The hologram reconstructions of Pediastrum (a,b) and Melosira (c,d) alga colonies without (a, c), and with (b, d) tilt compensation. (Scale bar is 20 μm).

The relative tilts (Θ) of the light reference beams and the reconstruction beams shows good matches as it was expected in the case of the tilt aberration. Also the properly corrected color images of algae are confirmed that our compensation method works correctly.

3.3 Numerical reconstruction issues

As we apply discrete Fourier transforms (fast Fourier transform) in the simulation of the wave field propagation, a tilted reconstructing beam can introduce phase discontinuity at the hologram borders. Such discontinuities will cause artificial diffractions at the hologram boundaries during the wave field propagation (see in Fig. 8. (b)). Although, there were attempts [30] to eliminate the effect of such discontinuities earlier, due to the special structure of the discontinuity introduced by the tilted reconstructing wave fields we propose here a new, simple, but efficient method.

With slight modification of the optimal wave number vector, which is able to compensate the tilt aberration perfectly, we can avoid the occurrence of this discontinuity. This modification is usually an order of magnitude smaller than the originally applied tilt compensation slopes; therefore it does not introduce any further color aberration.

To reconstruct an object using digital holography first we have to retrieve the complex wave field $E(x, y, 0)$ at the hologram plane. This can be done – aside from the zero order and twin image terms – by multiplying the measured intensity hologram $H(x, y)$ with the reference (reconstruction) wave field $R(x, y)$:

$$E(x, y, 0) = H(x, y) \cdot R(x, y). \tag{1}$$

As we described in the previous section this reconstruction wave field is unit intensity, appropriately tilted plane wave.

$$R(x, y) = 1 \cdot e^{i\phi} = e^{i\vec{r}\cdot\vec{k}} = e^{i(k_x \cdot x + k_y \cdot y)} \tag{2}$$

The wave number vector describes the actual tilt with k_x and k_y components.

If the applied reconstruction beam is parallel to the optical axis, then the x and y components of the wave vectors are zero. Otherwise, its values depend on the position of the illuminating light source and the parameters of the optical setup as it was detailed in the

#203656 - $15.00 USD Received 26 Dec 2013; revised 5 Feb 2014; accepted 8 Feb 2014; published 25 Mar 2014

previous section. The second step of the reconstruction of an object is the simulation of the wave propagation by the angular spectrum method [31, 32]. This method (and all the other methods) applies discrete Fourier transforms [31], that regards a periodic, infinite tiling of the wave field at the hologram plane as the input. We have no problem if these tiling is continuous at the hologram borders, otherwise large propagation artifacts emerge at the hologram boundaries. To avoid this, we have to eliminate these discontinuities at the borders of the hologram. This can be fulfilled evidently if the tilted wave field is periodic on the (padded [31]) hologram. The discontinuity introduced by the periodic tiling of the complex tilted reconstructing wave field is depicted in Fig. 8 (b). Here, the wave field is a plane wave with a slope that compensates the tilt aberration. The white line marks the boundaries of the padded hologram, while the 't', 'l', 'b', and 'r' (top, left, bottom and right) signs denotes how the different parts of the wave field are connected in an infinite periodic tiling. Slight modification of the plane wave slopes can restore the continuity at the boundaries as it is demonstrated in Fig. 8 (c). Phase continuity of the tiled hologram is assured if

$$\phi(x, y) = \phi(x + w, y) \quad \text{and} \quad \phi(x, y) = \phi(x, y + h) \tag{3}$$

hold for all the (x, y) points, where 'h' and 'w' corresponds to the height and width of the padded hologram.

This usually does not hold for arbitrary tilts. However, we can use an adapted wave vector

$$\bar{k}' = \bar{k} + \Delta\bar{k} \tag{4}$$

that satisfies Eq. (3) and where $\Delta\bar{k} \ll 1$.

In this case the displacement of the reconstructed color image shift remains discernible, while the periodicity of the wave vector is ensured. That is:

$$\begin{array}{ccc} e^{i(k_x'\cdot x + k_y'\cdot y)} & = & e^{i(k_x'\cdot (x+w) + k_y'\cdot y)} \\ e^{i(k_x'\cdot w)} & = & 1 \end{array} \quad \text{and} \quad \begin{array}{ccc} e^{i(k_x'\cdot x + k_y'\cdot y)} & = & e^{i(k_x'\cdot x + k_y'\cdot (y+h))} \\ e^{i(k_y'\cdot h)} & = & 1 \end{array}. \tag{5}$$

This holds, if

$$k_x' = N \cdot \frac{2\pi}{w} \quad \text{and} \quad k_y' = M \cdot \frac{2\pi}{h} \tag{6}$$

for some $N, M \in \mathbb{Z}$. In this case

$$\begin{gathered} \left|\Delta k_x\right| = \left|k_x' - k_x\right| = \left|N \times \frac{2\pi}{w} - k_x\right| \\ \text{and} \\ \left|\Delta k_y\right| = \left|k_y' - k_y\right| = \left|M \times \frac{2\pi}{h} - k_y\right|. \end{gathered} \tag{7}$$

$\left|\Delta k_x\right|$ and $\left|\Delta k_y\right|$ are minimal, if

$$\left|N - \frac{k_x \cdot w}{2\pi}\right| \quad \text{and} \quad \left|M - \frac{k_y \cdot h}{2\pi}\right| \tag{8}$$

are the smallest. This is the case, when

$$N = \text{round}\left(k_x \cdot \frac{w}{2\pi}\right) \quad \text{and} \quad M = \text{round}\left(k_y \cdot \frac{h}{2\pi}\right). \tag{9}$$

From this we get, that

#203656 - $15.00 USD Received 26 Dec 2013; revised 5 Feb 2014; accepted 8 Feb 2014; published 25 Mar 2014

$$k'_x = \text{round}\left(k_x \cdot \frac{w}{2\pi}\right)\frac{2\pi}{w} \quad \text{and} \quad k'_y = \text{round}\left(k_y \cdot \frac{h}{2\pi}\right)\frac{2\pi}{h}. \tag{10}$$

In our experiments the rounding errors were usually very small and result in sub pixel range shifts that do not disturb the correct, aligned color reconstructions. Furthermore, as only the relative angle of the different color illumination is relevant in the tilt correction, choosing a properly tilted reference beam direction the rounding errors, which can be large for small relative wave number vector components, can be further decreased.

In our experiments, the adapted wave vectors provide appropriate tilt compensated reconstructions and avoid the phase discontinuity caused propagation artifacts. We can compare the reconstructions of a simulated sample hologram (Fig. 8 (a)) without (Fig. 8 (d)) and with (Fig. 8 (e)) adapted tilt compensation.

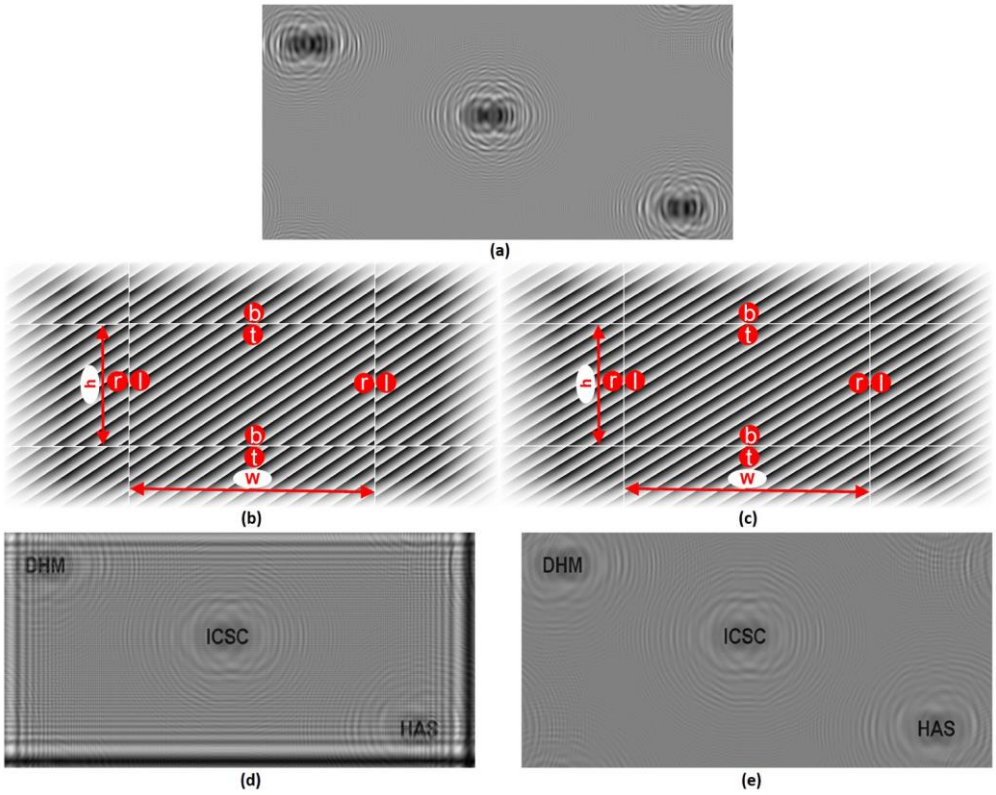

Fig. 8. Reconstruction from a digitally simulated sample in-line hologram (a), using a tilted reconstructing plane wave (b) shows considerable numerical reconstruction artifacts at the hologram borders (d). Discrete Fourier transform implies the infinite periodic tiling of the wave field. In the case of a tilted plane wave, this periodicity can introduce severe phase discontinuity (b) where the wave field and its copies meet at the border of the hologram. The **t**op, **l**eft, **b**ottom, and **r**ight borders are shown in the tiled copies, while 'w' and 'h' denotes the **w**idth and **h**eight of the detector respectively. The continuities of the phase at the detector boundaries can be ensured by slight modification of the applied plane wave slopes (c). Applying a reconstructing beam with this optimized tilt the artifact is perfectly eliminated (e).

4. Imaging performance of our color DHM

Using the introduced new kind of multicolor illumination and tilt aberration compensation in our color DHM device we obtain high quality, reconstructed color images of rarely occurring, freely floating microbiological objects from large fluid sample volumes. From a single acquired hologram the observable volume is ~1.5 mm^3 (where the field of view is ~1 mm^2

#203656 - $15.00 USD Received 26 Dec 2013; revised 5 Feb 2014; accepted 8 Feb 2014; published 25 Mar 2014

and the achieved lateral resolution is ~1 μm). The field of view of our system is confined by the field of view of the applied large working distance microscope objective. Eventually, the size of the applied sensor and the optical system define the achievable field of view together [17]. In our case the applied tilt aberration correction results in only a few pixels displacements of the different color reconstructions, thus it negligibly decreases the achievable field of view.

As we applied well corrected microscope objectives in our DHM there is no need of further color aberration corrections [33].

The imaging performance of our DHM is demonstrated by some hologram reconstructions (see in Fig. 9). The achievable resolution is measured and shown by a USAF test target, while the quality of the imaging is demonstrated by several sample color images of different reconstructed holograms of algae. In the reconstruction of USAF test target, group 8 is clearly, while group 9 is partially resolved, which is according to 0.75-1 μm lateral resolution.

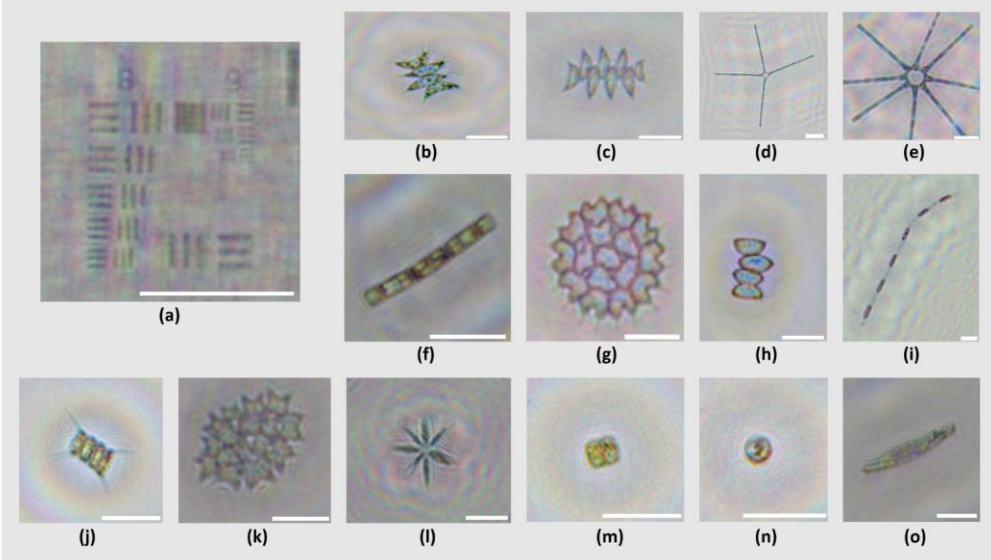

Fig. 9. Reconstruction of an USAF test target hologram (a) and some reconstructed color images of freely floating algae holograms. These algae are classified as Scenedesmus (b, c, h, j), Asterionella (d, e), Melosira (f, i), Pediastrum (g, k), Ankistrodesmus (l), Thalassiosirales (m, n), and Bacillariophyceae (o). (Scale bar is 20 μm.)

Due to the correct positioning of the different color hologram reconstructions the fine inner structures becomes clearly recognizable. Due to the multicolor hologram reconstruction, the otherwise apparent speckle and the twin image noises become less noticeable.

5. Conclusion

We introduced special, multicolor fiber coupled laser illumination assembly in our DHM. This device provides flexible, robust, stable, and compact illumination even in industrial environment. It is not difficult to apply, redesign, adjust in diverse optical holographic setups and it is simple to assemble in an optical lab using a standard optical fiber connectorizing kit. Its design avoids the otherwise always appearing coupling losses and it can provide high quality, regular, single mode Gaussian laser illuminating wave fields simultaneously at several different wavelengths.

We use a simple tilt aberration correction method to ensure proper alignment of the different color reconstructions. This can be used wherever the holograms are captured with the same optical setup or arrangement, but the applied illumination or reference waves have slightly different incident directions. Using properly tilted plane waves for the hologram

#203656 - $15.00 USD Received 26 Dec 2013; revised 5 Feb 2014; accepted 8 Feb 2014; published 25 Mar 2014

reconstruction process the positioning of the different color reconstructions becomes aligned wherever the actual reconstructed object position is within the volume.

In case of arbitrary tilted plane waves, phase discontinuities appear at the boundaries of the hologram and can cause numerical artifacts during the reconstruction. We introduced a simple method that ensures the continuity of the tilted plane wave phases at the tiled hologram boundaries and this way the artifact-free application of the discrete Fourier transformation becomes possible.

We applied this new type of illumination with the corresponding adapted tilt aberration correction methods in a DHM that is aiming high speed, volumetric microbiological water inspection. Using this holographic device we are able to achieve high quality, multicolor images of freely floating objects from a 1.5 mm^3 volume with 1 μm lateral resolution.

Appendix

One solution of the paraxial form of the Helmholtz equation is the Gaussian beam [27] that provides good approximation of the emitted wave field of lasers. Decentered Gaussian beam can be applied to describe the emitted wave field fiber coupled laser with displaced axis. We denote $\rho_g^2 = (x-x_0)^2 + (y-y_0)^2$ the squared axial distance, where the beam position is $(x_{0,}y_0)$. In this case the complex wave field can be written by:

$$\Phi(x,y,z) = A_0 \frac{w_0}{w(z)} \exp\left(-\frac{\rho_g^2}{w^2(z)} - i(kz - \zeta(z)) - ik\frac{\rho_g^2}{2R(z)} \right), \tag{A.1}$$

where $w(z) = w_0\left[1+\left(\frac{z}{z_0}\right)^2\right]^{1/2}$ is the spot size, $R(z) = z\left[1+\left(\frac{z_0}{z}\right)^2\right]$ is the radius of curvature and $\zeta(z) = \arctan\frac{z}{z_0}$ is the Gouy phase shift, while $w_0 = \left(\frac{\lambda z_0}{\pi}\right)^{1/2}$ is the waist size. Here, A_0 denotes the amplitude and z_0 the Rayleigh-range.

In the paraxial approximation, we can apply the ray transfer matrix (ABCD) formalism. Thus we get a modified Gaussian wave field as:

$$\Phi(x,y,z) = \frac{A_0}{A + B/q_0} \times \exp\left\{ -\frac{ik}{2q_1(z)}\left[(x-x_{01})^2 + (y-y_{01})^2\right] - ik(\varepsilon_{1x}x + \varepsilon_{1y}y) + i(\varphi_x + \varphi_y) \right\}, \tag{A.2}$$

where $q_1 = \frac{Aq_0 + B}{Cq_0 + D}$, $x_{01} = Ax_0$, $y_{01} = Ay_0$, $\varepsilon_{1x} = Cx_0$, $\varepsilon_{1y} = Cy_0$, $\varphi_x = \frac{kAC}{2}x_0^2$, $\varphi_y = \frac{kAC}{2}y_0^2$, and $q_0 = \frac{\pi w_0^2}{i\lambda}$, where w_0^2 is the square of the beam waist and λ is the wavelength.

The complex radius of curvature is defined by the radius of curvature $R(z)$, and the spot size $w^2(z)$:

$$\frac{1}{q(z)} = \frac{1}{R(z)} - i\frac{2}{kw^2(z)}. \tag{A.3}$$

Approximation of the phase distortion caused by the lateral displacement of the fiber-ends can be defined from these equations.

#203656 - $15.00 USD Received 26 Dec 2013; revised 5 Feb 2014; accepted 8 Feb 2014; published 25 Mar 2014

It is known, that the ABCD matrix of a lens with focal length f is $\begin{bmatrix} 1 & 0 \\ -\frac{1}{f} & 1 \end{bmatrix}$, while z distance free propagation can be described by $\begin{bmatrix} 1 & z \\ 0 & 1 \end{bmatrix}$. This way we can give the ABCD matrix of the applied actual optical setup.

Using two lenses and three free space propagation terms, we defined the following ABCD matrix:

$$\begin{bmatrix} A & B \\ C & D \end{bmatrix} = \begin{bmatrix} 1 & z_2 \\ 0 & 1 \end{bmatrix} \begin{bmatrix} 1 & 0 \\ -\frac{1}{f_2} & 1 \end{bmatrix} \begin{bmatrix} 1 & d \\ 0 & 1 \end{bmatrix} \begin{bmatrix} 1 & 0 \\ -\frac{1}{f_1} & 1 \end{bmatrix} \begin{bmatrix} 1 & z_1 \\ 0 & 1 \end{bmatrix}, \tag{A.4}$$

where z_1, z_2, and d are the distance of the laser source from the first objective (which is considered to be a thin lens in this approximation), the distance of the second objective lens and the sensor surface, and the distance of the two objectives, respectively, while f_1, f_2 correspond to the focal lengths of the applied objectives.

After short calculations, the elements of the matrix are:

$$\begin{aligned} A &= 1 - \frac{z_2}{f_2} - \left(\left(1 - \frac{z_2}{f_2} \right) d + z_2 \right) \frac{1}{f_1}, \\ B &= A z_1 + \left(1 - \frac{z_2}{f_2} \right) d + z_2, \\ C &= -\frac{1}{f_2} - \left(1 - \frac{d}{f_2} \right) \frac{1}{f_1}, \\ D &= C z_1 - \frac{d}{f_2} + 1. \end{aligned} \tag{A.5}$$

In an afocal system the distance d between the objective and tube lens is: $d = f_1 + f_2$. This way, in our case three elements of the matrix become simpler:

$$A = 1 - \frac{d}{f_1}, \quad C = 0, \quad \text{and} \quad D = 1 - \frac{d}{f_2}. \tag{A.6}$$

The Gaussian beam can be characterized by the use of the radius parameter of the complex curvature [34] Eq. (A.7).

$$F(r,z) = \frac{1}{q(z)} \exp\left\{ -ik \frac{r^2}{2q(z)} \right\} \tag{A.7}$$

where $r^2 = x^2 + y^2$. This way, we can get the parameters of the Gaussian beam, which is propagated through the ABCD matrix system. The complex radius of curvature $q'(z)$ (see in Eq. (A.3)) of the beam after the optical system is defined in Eq. (A.8):

$$q'(z) = \frac{Aq(z) + B}{Cq(z) + D}. \tag{A.8}$$

The exponent of the Eq. (A.7) gives the phase term of the propagated wave. Taking the first order part of the Taylor expansion of the phase term, we get the phase tilt. The real part of the

#203656 - $15.00 USD Received 26 Dec 2013; revised 5 Feb 2014; accepted 8 Feb 2014; published 25 Mar 2014

phase tilt substituted by Ar_0 leads to a wave number which describes the tilted plane wave as it is shown in Eq. (A.9).

$$k = R\left(\frac{1}{q'(z)}\right)\frac{2pAr_0}{l}. \tag{A.9}$$

In Subsection 3.2, the relative angles were calculated using Eq. (A.9), applying the measured distances of the red fiber end from the other two (r_{ob}, r_{og}) and the parameters of the optical system besides the corresponding wavelengths.

Acknowledgments

This work was funded by the Hungarian National Office for Research and Technology (NKTH 1981822A) project entitled "Water Biology Digital Holographic Microscope (DHM) as an early warning environmental system."